2008 American Control Conference
Westin Seattle Hotel, Seattle, Washington, USA
June 11-13, 2008

Model-Based Predictive Control of an Electro-Pneumatic Exhaust Valve for Internal Combustion Engines

Jia Ma, Guoming Zhu, Andrew Hartsig, and Harold Schock

Abstract— **Variable valve actuation of Internal Combustion (IC) engines is capable of significantly improving their performance. Variable valve actuation can be divided into two main categories: variable valve timing with cam shaft(s) and camless valve actuation. For camless valve actuation, research has been centered in electro-magnetic, electro-hydraulic, and electro-pneumatic valve actuators. This research studies the control of the electro-pneumatic valve actuator. The modeling and control of intake valves for the Electro-Pneumatic Valve Actuators (EPVA) was shown in early publications and this paper extends the EPVA modeling and control development to exhaust valves for both valve timing and lift control. The control strategy developed utilizes model-based predictive techniques to overcome the randomly variable in-cylinder pressure against which the exhaust valve opens.**

I. INTRODUCTION

Variable intake valve timing and lift can be used to optimize engine performance over a wide operating range, for instance, to reduce engine pumping losses, deactivate selected cylinder(s), and control flame speed by manipulating in-cylinder turbulence. Exhaust valve timing and lift control makes it possible to vary the amount of Residual Gas Recirculation (RGR) and control valve overlap when combined with intake valve control. Variable valve timing and lift control is also a key technology for HCCI (Homogenous Charge Compression Ignition) combustion control.

Variable valve actuation can be achieved with mechanical (cam-based), electro-magnetic (electric mechanical), electro-hydraulic, and electro-pneumatic valvetrain mechanisms. The cam-based variable valve actuation is able to provide either a multiple stepping or a continuously changing valve timing phase shift. See [1], [2] and [3]. Infinitely variable valvetrain, often referred to as camless valvetrain, includes electro-magnetic ([4], [5], [6], [7], and [8]), electro-hydraulic ([9] [10] and [11]), and electro-pneumatic actuation ([12]). The electro-pneumatic valve actuator (EPVA) utilizes the supplied air pressure to actuate either the intake or exhaust valve by electronically controlling solenoids that control the motion of the actuator's piston. For both electro-hydraulic and electro-pneumatic valves, there is a potential issue of having a repeatable valve lift over the life of an engine.

Valve lift control for electro-hydraulic valvetrain actuation has been investigated by a number of researchers. Adaptive peak lift control was presented in [15], and digital valve technology was applied to control of a hydraulic valve actuator in [17]. The modeling and control of intake valves for the electro-pneumatic valve actuators was shown in [12], [13] and [14].

Unlike the intake valve, the exhaust valve opens against an in-cylinder pressure that varies as a function of the engine operational conditions with cycle-to-cycle combustion variations. This pressure disturbance slows down the valve actuator response and as a result, it increases the variation of valve opening delay. In fact, this disturbance makes it difficult to maintain repeatable valve opening timing and lift. As a result, unrepeatable valve lift affects the closing timing control which is critical for RGR control. Therefore, this work addresses exhaust valve lift control.

A mathematical in-cylinder pressure model at exhaust opening was developed and integrated with the exhaust valve model for control development. The thermodynamics data was obtained using WAVE^{TM} simulation [20]. The WAVE^{TM} model was calibrated and validated using experimental in-cylinder pressure data. The mathematical in-cylinder pressure model is then used to develop the model-based predictive control scheme for exhaust valve lift. The controller consists of two parts: feedforward and closed loop controls. The feedforward control is used to provide a nominal lift control based upon the predicted valve opening trajectory, while the closed loop controller is used to minimize the mean control error. The closed-loop control strategy was developed and verified in simulation using the combined mathematical model of exhaust valve and in-cylinder pressure.

The paper is organized as follows. First, an exhaust valve dynamic model is presented in Section II. Next, the feedforward and closed loop control strategies are discussed in Section III. Third, the simulation validation results are shown in Section IV, and finally, conclusions are drawn.

II. EXHAUST VALVE DYNAMIC MODEL

A physics-based nonlinear model, called a level one model, was built component-by-component based upon the flow and fluid dynamics. The details of the level one model and its verification can be found in [12]. This model provides an insight to the operation of the pneumatic/hydraulic mechanical actuation system. A piecewise linearized level two model was then created based on the level one model to reduce the computational throughput for control system development purposes. The details of the level two model are described in [13]. The level two model was used as

This work was supported by Department of Energy

Jia Ma is with Delphi Corporation. This work was completed as part of her Ph.D. study at Michigan State University, USA jia.ma@delphi.com

Guoming Zhu, Andrew Hartsig, and Harold Schock are with Mechanical Engineering, Michigan State University, Engineering Research Complex South, East Lansing, MI 48824, USA zhug@egr.msu.edu, hartsiga@msu.edu and schock@egr.msu.edu

the actuator model for the intake valve in the previous studies. Here, it is used for the exhaust valve actuator modeling. The exhaust valve opens against a high in-cylinder combustion pressure with large cycle-to-cycle variations. This in-cylinder pressure produces a force on the face of the exhaust valve that affects the valve dynamics. This in-cylinder pressure is modeled and integrated with the exhaust valve actuator model to capture the exhaust valve dynamics. The system dynamics illustrated here focuses

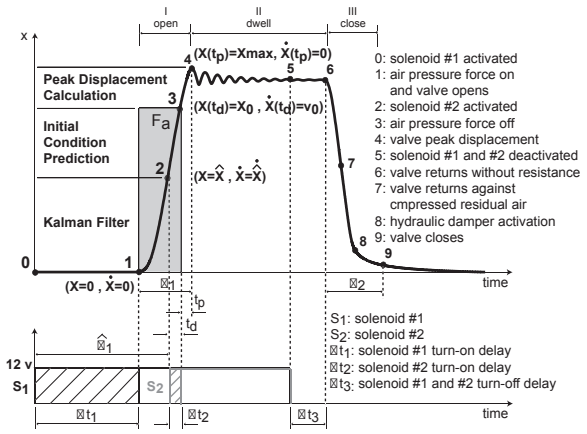

Fig. 1. Valve lift profile with the solenoid command chart and exhaust valve lift control strategy

on the relationship between the solenoid control commands and the exhaust valve response. It follows the same analysis as that of the level two model which simplifies the system dynamics used for the level one model analysis. As shown in Figure 1, the valve response can be divided into three stages. They are the opening stage (I), dwell stage (II), and closing stage (III). Solenoid $\#1$ is activated at point 0 first. It induces a high air pressure force to push the valve open at point 1 after Δt_1. Solenoid $\#2$ is then activated (point 2) with a time lag $\hat{\delta}_1$. It removes this air pressure force Δt_2 time after solenoid $\#2$ is activated (point $\#3$). Note that the interplay between two solenoids results in a pulse force input to the actuator valve piston with pulse width δ_1 between points 1 and 3. The increment of the pulse width increases valve lift. Now, with zero input, the valve movement continues until it reaches its peak lift at point $\#4$, the valve equilibrium. This ends the open stage. Next, the valve enters the dwell stage where it is held open by a hydraulic latch mechanism. At the end of the dwell stage, solenoid $\#1$ is deactivated at point $\#5$. After Δt_3 time, the valve starts to return (point $\#6$). The close stage starts at point $\#6$ and ends at point $\#9$ where the valve is considered closed. The returning duration is δ_2 between these two points.

The two solenoids have electro-mechanical delays after their activation and de-activation (see Figure 1). Δt_1 is defined as the delays for solenoid $\#1$ at activation. Δt_2 is defined as solenoid $\#2$ delay at activation. The de-activation delay for both solenoids are Δt_3. The solenoid commands direct the valve motion after the delays. The time lag applied between the activation of two solenoids is denoted as $\hat{\delta}_1$. This differs from the time lag between two delayed solenoid activations which is denoted as δ_1 since two solenoid delays, Δt_1 and Δt_2, are not equal. The exhaust valve lift control algorithm is to determine when to activate solenoid $\#2$ during exhaust valve opening for each cycle with the varying in-cylinder pressure at the face of the valve and its activation delay in presence. It is impossible to remove the input force F_a instantly upon the activation of solenoid $\#2$ due to its activation delay. An model-based predictive lift control algorithm is developed to make this possible. The details are described in the control strategy section.

The exhaust valve closing timing control requires knowledge of δ_2, the amount of time that the valve takes to close. To guarantee the exhaust valve closing at the desired time requires de-activating solenoid $\#1$ by time δ_2 before exhaust valve closing. δ_2 can be predetermined from the different valve lift set points. In other words, the closing timing control relies on a repeatable valve lift control. Developing a lift control system is the primary emphasis of work described in this paper.

The opening stage exhaust valve actuator model and the in-cylinder pressure model are employed to formulate the model-based predictive lift control scheme. In order to validate the exhaust valve lift control algorithm, the level two model integrated with the in-cylinder pressure model is used as a plant model in simulation. The opening stage exhaust valve actuator model and the in-cylinder pressure model are introduced in the following two subsections.

A. Actuator Model

The opening stage exhaust actuator model with the in-cylinder pressure is studied in this section. This model is expanded based on the level two model [13] to include the in-cylinder pressure dynamics. Figure 2 shows the

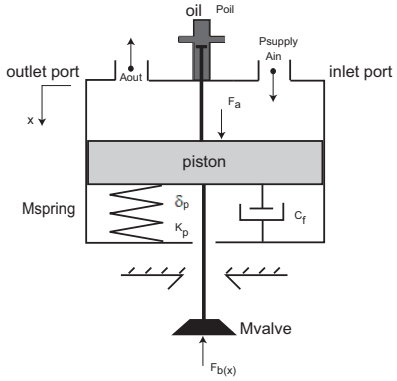

Fig. 2. Actuator piston model

schematic diagram of a single actuating piston for this system. At the opening stage, the valve actuator is modeled as a second order mass-spring-damper system with zero initial conditions. See Equation (1). All pressures used in modeling and control formulation process are gauge pressure in this article.

$$M\ddot{x} + C_f\dot{x} + K_p(x + \delta_p) = F_a(t) - F_b(x) \qquad (1)$$

$$F_a(t) = F(t) - F(t - \delta_1), F(t) = \begin{cases} 0, & t < 0 \\ A_p P_p, & t \geq 0 \end{cases} \qquad (2)$$

where, P_p is supply air pressure; $F_b(x)$ is the in-cylinder pressure force applied at the back of the exhaust valve; M is the equivalent mass of actuator piston, effective valve spring mass [18], exhaust valve and cap; A_p is the sum of actuator piston and oil passage areas; C_f is the damping ratio approximating energy dissipation due to flow loss and frictional loss; K_p and δ_p are the stiffness and preload of the valve spring respectively; δ_1 is the lag between the activation of solenoids $\#1$ and $\#2$ after solenoid delays as shown in Figure 1.

B. In-cylinder Pressure Model

The in-cylinder pressure $F_b(x)$ needs to be modeled and evaluated in Equation (1). Figure 3 illustrates the dynamics in the combustion chamber with an exhaust valve. A control volume is drawn above the piston, where m_{cyl}, T_{cyl} and P_{cyl} are the mass, temperature and pressure inside the combustion cylinder. A_{cyl} is the engine piston area. $\dot{m}_{ex}$ is the mass flow rate at the exit when the exhaust valve opens. T_{atm} and P_{atm} are the atmospheric temperature and pressure. x and y are the exhaust valve displacement and cylinder piston displacement respectively. The mass flow rate equations at

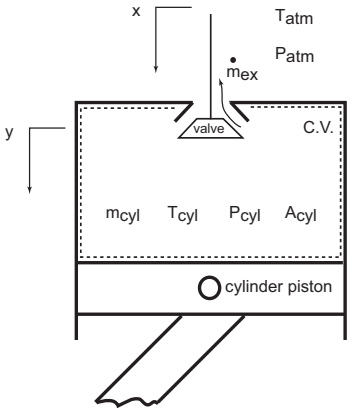

Fig. 3. In-cylinder pressure model

the exit are written for both choked and unchoked flow cases through Equations (3) to (5) following their derivation in [16].

$$\dot{m}_{ex} = C_{d_{ex}} \gamma P_{cyl} A_{ex}(x) \sqrt{\frac{k}{RT_{cyl}}},\ A_{ex} = 2\pi r_{valve} x, \quad (3)$$

where, A_{ex} is the flow area with r_{valve} being the valve radius; $C_{d_{ex}}$ is the flow coefficient at the exit; and R is the residual gas constant. C_p and C_v are the specific heat of the residual gas at constant pressure and constant volume respectively; and $k = \frac{C_p}{C_v}$. When $P_{cyl} \geq (\frac{k+1}{2})^{\frac{k}{k-1}} P_{atm}$, the flow is choked at the exit. In this case, γ is shown in Equation (4)

$$\gamma = \sqrt{(\frac{2}{k+1})^{\frac{k+1}{k-1}}}. \quad (4)$$

When $P_{cyl} \leq (\frac{k+1}{2})^{\frac{k}{k-1}} P_{atm}$, the flow is unchoked and γ is expressed in Equation (5).

$$\gamma = \sqrt{\frac{2}{k-1}(\frac{P_{atm}}{P_{cyl}})^{\frac{k+1}{2k}}[(\frac{P_{atm}}{P_{cyl}})^{\frac{1-k}{k}} - 1]}. \quad (5)$$

The mass of the residual gas inside the combustion cylinder in Equation (6) can be obtained by integrating the calculated mass flow rate. The initial mass m_0 is derived using ideal gas law in Equation (6):

$$m_{cyl} = -\int_0^t \dot{m}_{ex} dt + m_0, \quad m_0 = \frac{P_0 V_0}{R T_{cyl_0}}. \quad (6)$$

where P_0, V_0, R_0 and T_{cyl_0} are the initial in-cylinder gas pressure, volume, gas constant and temperature at the exhaust valve opening. Using the ideal gas law again with the obtained m_{cyl} results in an expression of in-cylinder pressure as shown in Equation (7).

$$P_{cyl} = \frac{m_{cyl} R T_{cyl}}{V_{cyl}}, \quad V_{cyl} = A_{cyl} y, \quad (7)$$

where, k, R and T_{cyl} are variables acquired from the WAVE^{TM} simulation with the same engine configuration and parameters; and y is the piston displacement derived from the cylinder geometry in Equation (8).

$$y = r[1 + \frac{L}{r} - \cos(\theta) - \sqrt{\frac{L}{r} - \sin^2(\theta)}], \quad (8)$$

where

- $A_{cyl} = \pi(\frac{1}{2} \times bore)^2 = 0.0401 m^2$ ($bore = 90.2mm$) ,
- L is the connecting rod length ($L = 169.2mm$),
- r is the crank shaft radius ($r = \frac{1}{2} stroke = 52.9mm$),
- θ is the engine crank angle.

Therefore, $F_b(x)$ can be expressed in Equation (9) below.

$$F_b(x) = P_{cyl} A_{valve}, \quad (9)$$

where P_{cyl} is defined in Equation (7).

C. Validation of In-cylinder Pressure Model by Simulation

The in-cylinder pressure force F_b is a function of the effective flow out area A_{ex} which varies as the exhaust valve displacement cahnges.

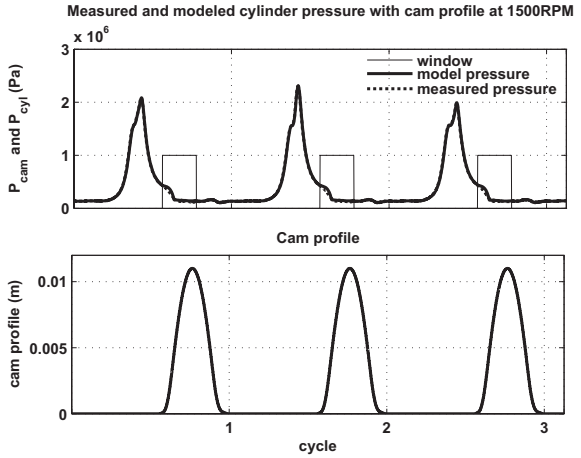

Fig. 4. In-cylinder pressure model validation by simulation

In order to validate the in-cylinder pressure model, combustion experiments were conducted using a 5.4L 3 valve V8 engine with in-cylinder pressure measurement and a conventional camshaft at 1500RPM. The pressure model

was simulated using the conventional cam profile as the valve displacement input. The modeled in-cylinder pressure was then compared with the measured in-cylinder pressure as shown in Figure 4. The top diagram of this figure shows the modeled pressure (solid line) in the rectangular windows and measured in-cylinder pressure (dash line) with satisfactory modeling accuracy. The bottom diagram shows the exhaust cam profile used in the simulation and experiments. The in-cylinder pressure model is then integrated into the pneumatic exhaust valve model and the responses are shown in Figure 5. Here, the pressure model uses the EPVA valve displacement to calculate the corresponding in-cylinder pressure. The modeled pressure (solid line in top diagram) and the associated EPVA valve lift profile (solid line in bottom diagram) are compared with the experiment pressure (dash line) and the cam profile (dash line). The simulation result demonstrates that the in-cylinder pressure drops rather quickly with the EPVA exhaust valve actuation since the EPVA valve opens faster than the conventional cam-based valve. This simulated in-cylinder pressure is used to construct the control signals. The exhaust valve model is used as a plant model and it is integrated with the in-cylinder pressure model in simulations to validate the control algorithm. The modeled in-cylinder pressure is one of the two inputs to the plant (exhaust valve), and the actuation force F_a commanded by the two solenoid control signals is the other input.

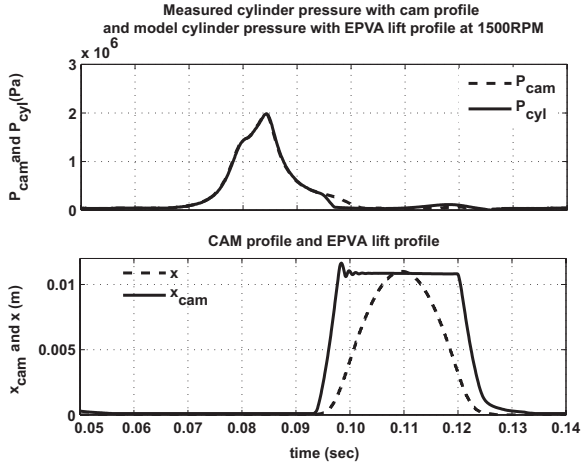

Fig. 5. In-cylinder pressure model integrated into exhaust valve model

III. CONTROL STRATEGY

Since the in-cylinder pressure on the face of the exhaust valve varies significantly from cycle-to-cycle, the valve lift control needs to be adjusted as a function of the current in-cylinder pressure for each individual cycle. As explained in the actuator dynamics section, the exhaust actuator is modeled as a second order mass-spring-damper system at the opening stage. Activating solenoid $\#1$ applies the force F_a on the valve and moves the exhaust valve. Activating solenoid $\#2$ removes the force and the valve continues to open until it reaches the maximum displacement. Solenoid $\#2$ activation timing determines the maximum valve lift. Therefore, the key for valve lift control is to find when to activate solenoid $\#2$. Figure 1 illustrates the idea of the exhaust valve lift control strategy. Solenoid $\#1$ is activated at time 0. After the delay of Δt_1, the input force F_a acts on the system and the exhaust valve starts to open at point 1. Solenoid $\#2$ is then activated at point 2. After Δt_2 delay, force F_a is removed at point 3. The valve moves further until its velocity decreases to 0 at point 4. The second order valve system response from points 3 to 4 can be calculated with zero input and nonzero initial conditions at point 3. In other words, the valve peak displacement at point 4 can be calculated if the initial displacement and velocity at point 3 are known. Once the calculated displacement at point 4 reaches the reference maximum valve lift, point 3 is found to be the right time to remove force F_a. If activating solenoid $\#2$ could turn off the input force F_a immediately, we would only need to activate it whenever the calculated displacement of point 4 reaches the reference lift. But the solenoid delay requires the activation to take place at point 2 with Δt_2 amount of time before point 3. This means that if point 3 is the time to eliminate input force, point 2 is the time to activate solenoid $\#2$. However, the initial conditions at point 3, where the peak displacement of the valve is calculated, are not yet available at point 2. Therefore, an algorithm is derived to predict initial conditions of point 3 at point 2. This strategy of initial condition prediction can be implemented as long as the delay Δt_2 of solenoid $\#2$ is less than the lag $\hat{\delta}_1$ between the activation of two solenoids. The predictive algorithm needs to know both states, valve displacement and velocity, at point 2. A Kalman state estimator was used to estimate them with minimized effect of measurement noise. Now we can determine the time to activate solenoid $\#2$ (point 2), which is served as a feedforward control of the valve actuator. A proportional and integral (PI) scheme is used as a closed-loop feedback lift control system to reduce the steady state lift tracking error.

The flow chart of the feedforward control scheme is shown in Figure 6. First, solenoid $\#1$ is activated. Secondly, the Kalman state estimator provides the current states. Finally, a model-based prediction algorithm uses the estimated states to calculate the states after solenoid $\#2$ delay Δt_2, which is then used to calculate the peak valve displacement. If the calculated peak displacement is greater than or equal to the reference valve lift, solenoid $\#2$ is activated, otherwise, the process repeats until the condition is satisfied. The details of the derivations are discussed in the following four subsections.

A. Peak Displacement Calculation (PDC)

This section describes the solution for the peak displacement at point 4 based on the initial conditions at point 3. Recall that the governing equation of the exhaust valve at the opening stage is presented in Equation (1). The back pressure force $F_b(x)$ equals the product of the exhaust valve area and the modeled in-cylinder pressure. The in-cylinder pressure used in the control algorithm development here is piece-wisely linearized between points 1 and 4 according

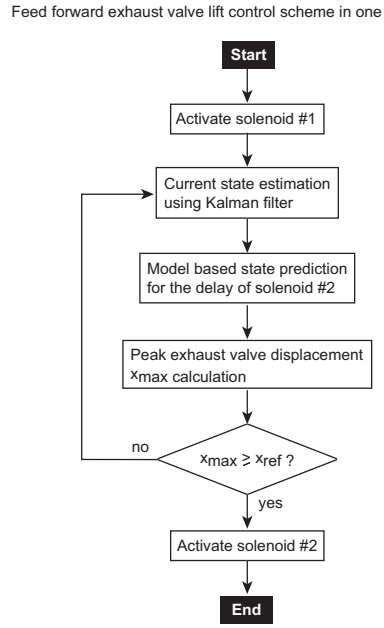

Fig. 6. Feedforward exhaust valve lift control strategy

to the simulated in-cylinder pressure against EPVA exhaust valve profile. Three lines were used for piecewise approximatation of the in-cylinder pressure data, and $F_b(x) = px+q$ ($p \leq 0$ and $q \geq 0$) with

$$\begin{cases} p = p_1,\ q = q_1,\ \ x \leq 0.002m \\ p = p_2,\ q = q_2,\ \ 0.002m < x \leq 0.008m \\ p = p_3,\ q = q_3,\ \ x > 0.008m \end{cases}.$$

Substituting $F_b(x)$ with its linearized expression into Equation (1) results in Equation (10) below.

$$M\ddot{x} + C_f\dot{x} + K_p x = F_a - (px + q) - K_p\delta_p. \quad (10)$$

Move the px term to the left resulting in Equation (11):

$$M\ddot{x} + C_f\dot{x} + (K_p + p)x = F_a - q - K_p\delta_p. \quad (11)$$

Let $K = K_p + p$ and $F_a = 0$, since it is assumed that input force F_a is turned off, to obtain Equation (12) in a general format given the initial condition $x(0) = x_0,\ \dot{x}(0) = v_0$.

$$M\ddot{x} + C_f\dot{x} + Kx = -Q,\ Q = K_p\delta_p + q. \quad (12)$$

Recall that p takes three different values, p_1, p_2 and p_3 in three valve displacement regions. K could be either negative, zero or positive depending on the value of p. When K is positive, Equation (12) can be rewritten into Equation (13) as below:

$$\ddot{x} + 2\zeta\omega_n\dot{x} + \omega_n^2 x = -\frac{Q}{M}, \quad (13)$$

where $\omega_n = \sqrt{\frac{K}{M}}$ and $\zeta = \frac{C_f}{2}\sqrt{\frac{1}{MK}}$. In this case, the solution can be categorized into under damped, critically damped and over damped scenarios depending on the value damping ratio ζ, damping coefficient C_f, mass M and equivalent stiffness K in Equation (13). The peak displacement solution derivation of Equation (12) proceeds separately in four cases. They are $K > 0$ with $0 < \zeta < 1$ (case #1), $K > 0$ with $\zeta = 1$ (case #2), $K > 0$ with $\zeta > 1$ (case #3) and $K \leq 0$ (case #4). The initial condition denoted as $x(0) = x_0$ and $\dot{x}(0) = v_0$ in this section are derived in the next section of model-based initial condition prediction.

For under damped PDC case #1 ($K > 0$ and $0 < \zeta < 1$), we start with solving Equation (13) for all three cases where $K > 0$. The homogenous solution x_h can be expressed in Equation (14)

$$x_h = e^{-\zeta\omega_n t}(a_1 e^{i\omega_d t} + a_2 e^{-i\omega_d t}),\ \omega_d = \sqrt{1-\zeta^2}\omega_n. \quad (14)$$

Solving for the particular solution x_p of Equation (13) results in Equation (15)

$$x_p = -\frac{Q}{K}. \quad (15)$$

The complete solution $x(t) = x_p(t) + x_h(t)$ can be expressed in Equation (16).

$$x(t) = e^{-\zeta\omega_n t}(a_1 e^{i\omega_d t} + a_2 e^{-i\omega_d t}) - \frac{Q}{K}. \quad (16)$$

We apply Euler formula $e^{i\alpha} = cos(\alpha) + isin(\alpha)$ and trigonometric identities to the equation above to obtain Equation (17)

$$x(t) = Ae^{-\zeta\omega_n t}\sin(\omega_d t + \theta) - \frac{Q}{K}, \quad (17)$$

where A and θ are determined by the initial conditions as follows:

$$\begin{cases} x(0) = A\sin(\theta) - \frac{Q}{K} = x_0 \\ \dot{x}(0) = -\zeta A\omega_n\sin(\theta) + \omega_d A\cos(\theta) = v_0, \end{cases}$$

$$\begin{cases} A = \sqrt{\frac{(v_0+\zeta\omega_n\chi_0)^2 + \chi_0^2\omega_d^2}{\omega_d^2}}, \chi_0 = x_0 + \frac{Q}{K} \\ \theta = tan^{-1}(\frac{\omega_d\chi_0}{v_0+\zeta\omega_n\chi_0}). \end{cases}$$

The peak displacement $x_p = x(t_p)$ is solved at $\dot{x}(t_p) = 0$ with t_p being the time the valve takes to travel to its maximum displacement (see Figure 1). Taking the time derivative of $x(t)$ and setting it to zero at t_p results in Equation (18).

$$\dot{x}(t_p) = -\zeta\omega_n A e^{-\zeta\omega_n t_p}\sin(\omega_d t_p + \theta) = 0. \quad (18)$$

Solving Equation (18) yields:

$$t_p = \begin{cases} \frac{1}{\omega_d}\left(tan^{-1}(\sqrt{\frac{1}{\zeta^2}-1}) - \theta\right), & tan^{-1}\sqrt{\frac{1}{\zeta^2}-1} > \theta \\ \frac{1}{\omega_d}\left(tan^{-1}(\sqrt{\frac{1}{\zeta^2}-1}) - \theta + 2\pi\right), & otherwise. \end{cases}$$

We substitute t_p into Equation (17) to obtain the peak displacement $x(t_p)$. The solution of the peak displacement is summarized below:

PDC Summary $K > 0$ with $0 < \zeta < 1$
$x(t_p) = Ae^{-\zeta\omega_n t_f}\sin(\omega_d t_p + \theta) - \frac{Q}{K}$ $Q = K_p\delta_p + q,\ K = K_p + p,\ \theta = tan^{-1}(\frac{\omega_d\chi_0}{v_0+\zeta\omega_n\chi_0})$ where, $x_0 = x(t_d),\ v_0 = \dot{x}(t_d)$, $x(t_d)$ and $\dot{x}(t_d)$ are from model-based initial condition prediction

For PDC cases #2, #3, and #4, the results can be derived similarly and are omitted in this paper.

B. Model-Based Initial Condition Prediction (ICP)

The previous section solves for the peak displacement $x(t_p)$ using the displacement and velocity at point 3 as initial conditions (Figure 1). This section derives the formulas to predict the displacement $x(t_d)$ and velocity $\dot{x}(t_d)$ at point 3, given the displacement and velocity at point 2. The displacement and velocity at point 2 are initial conditions denoted as $x(0) = x_0$ and $\dot{x}(0) = v_0$ in this subsection. Their values are estimated by the Kalman state estimator described in the next subsection. Solenoid #2 delay, Δt_2, is the time input and F_a is a constant force input between points 2 and 3. Consider the governing equation again in Equation (1). Given $F_b(x) = px + q$, Equation (1) becomes

$$M\ddot{x} + C_f\dot{x} + K_p x = F_a - (px + q) - K_p\delta_p. \tag{19}$$

Rearrange the equation above to obtain

$$M\ddot{x} + C_f\dot{x} + (K_p + p)x = F_a - q - K_p\delta_p. \tag{20}$$

Let $K = K_p + p$ and $W = q + K_p\delta_p - F_a$, Equation (20) becomes Equation (21).

$$M\ddot{x} + C_f\dot{x} + Kx = -W. \tag{21}$$

It is clear that Equations (12) and (21) have the same form. Previously, Equation (12) was evaluated for the maximum displacement given initial conditions. Now, Equation (21) is evaluated for the displacement and velocity in t_d amount of time with given initial conditions, where $t_d = \Delta t_2$ (see Figure 1). Equation (21) can be solved in a similar way to Equation (12) by replacing Q with W, and the solutions are omitted in this paper.

C. Kalman Filter State Estimation (KFE)

The displacement and velocity at point 2 (see Figure 1) are needed as initial conditions in the previous section. The system is equipped with a displacement sensor which measures the exhaust valve displacement. The velocity obtained through taking a time derivative of the measured displacement is unreliable due to the measurement noise. The observer formulated in this section performs the optimal estimations of both the displacement and velocity at point 2 in the presence of noise using the Kalman state estimator. The estimated displacement and velocity are denoted as $\widehat{x}$ and $\dot{\widehat{x}}$ respectively. The state space notation of the system is expressed below:

$$\begin{aligned} \dot{x} &= Ax + Bu + Gw(t) \\ y &= Cx + v(t) \end{aligned}$$

where $A = \begin{bmatrix} 0 & 1 \\ \frac{-K}{M} & \frac{-C_f}{M} \end{bmatrix}$, $B = \begin{bmatrix} 0 \\ 1 \end{bmatrix}$, $C = \begin{bmatrix} 1 & 0 \end{bmatrix}$ and $x^T = [x_1, x_2]$; $w(t)$ and $v(t)$ represent the process noise and measurement noise. Note that $u = -W$ is the input to the system, $x_1 = x$ and $x_2 = \dot{x}$ are the states representing the valve displacement and velocity. The Kalman state estimator takes the following forms:

$$\begin{aligned} \dot{\widehat{x}} &= A\widehat{x} + Bu + L(y - c\widehat{x}) \\ y &= C\widehat{x}, \quad \widehat{x}(0) = 0, \end{aligned}$$

where L is the observer gain acquired through solving the algebraic Riccati Equation (22); and $\widehat{x}$ is the estimated displacement x_1 and velocity x_2; and G is an identity matrix.

$$AP + PA^T + GWG^T - PC^TV^{-1}CP = 0, \tag{22}$$

$$L = PC^TV^{-1}, where\ W \geq 0\ and\ V > 0, \tag{23}$$

where W and V are covariance matrices of w and v, respectively. If (C, A) is observable, the algebraic Riccati equation has a unique positive definite solution P, and the estimated state $\widehat{x}$ asymptotically approaches true state x.

D. Closed-Loop Control Scheme

The feedforward solution of solenoid #2 activation timing is obtained by implementing the formulas from the peak displacement calculation, model-based initial condition prediction and Kalman filter state estimation subsections. This solution combined with the displacement error compensation from the proportional and integral (PI) feedback scheme forms a closed-loop control signal of solenoid #2 as illustrated in Figure 7.

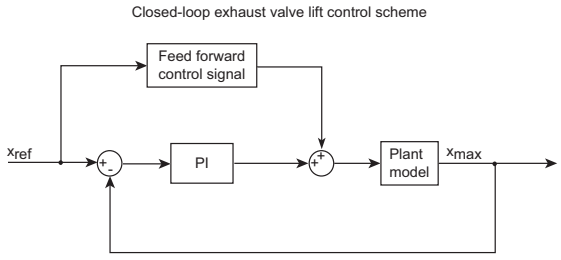

Fig. 7. Closed-loop exhaust valve lift control scheme

IV. SIMULATION RESULT

The developed control algorithms are validated by simulation using the combined valve actuator and the in-cylinder pressure model as the plant model. The three segments of the feedforward control strategy and the closed-loop control scheme are evaluated in sequence.

A. Simulation of Peak Displacement Calculation

Figure 8 demonstrates the simulation results in four out of 80 cycles, where the solenoid #2 is activated when the calculated peak displacement reaches the reference valve peak lift of $11mm$. This tests the open loop feedforward peak displacement calculation algorithm. The model valve displacement and velocity are employed as the known initial condition in this simulation. The top diagram shows that the peak valve lift is maintained at $11mm$, rejecting the in-cylinder pressure variation at the back of the exhaust valve (shown in the bottom diagram) when the feedforward peak displacement calculation is applied.

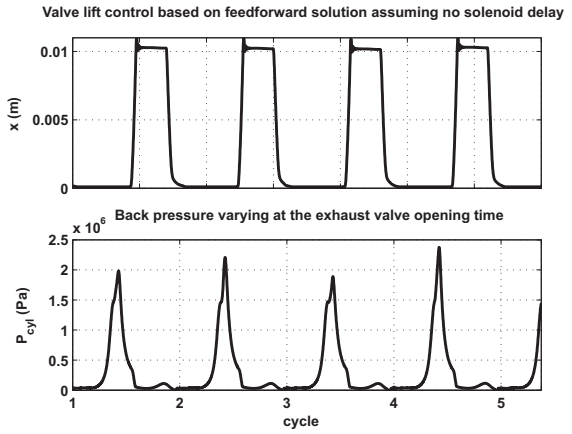

Fig. 8. Feedforward solution simulation without solenoid #2 delay

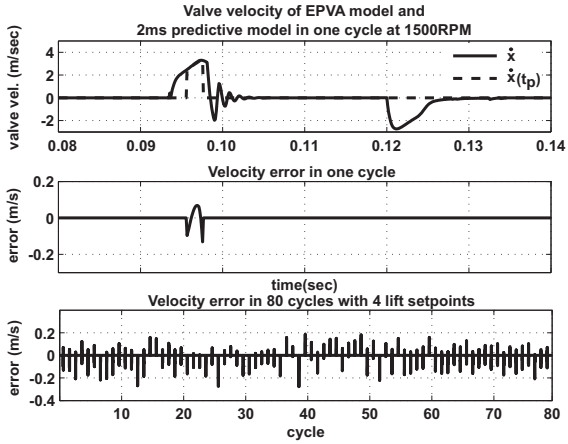

Fig. 10. Simulation validation of velocity prediction $\dot{x}_{0_p}$

B. Simulation of Model-Based Initial Condition Prediction

Figure 9 presents the simulation results of the model-based displacement prediction. The solenoid $\#2$ delay (Δt_2 or t_d) is assumed to be $2ms$ in the simulation. White noise is injected to the plant displacement output to simulate the measurement noise. The plant displacement (solid line) without measurement noise and the predicted displacement (dash line) in the prediction active region are displayed in the top diagram for one cycle. The middle diagram displays the error between the two. The bottom diagram shows the tracking error between the plant and predicted displacement. The lift set points were selected as $11mm$, $6mm$, $8mm$, and again $11mm$. The absolute error is less than $0.7mm$. The

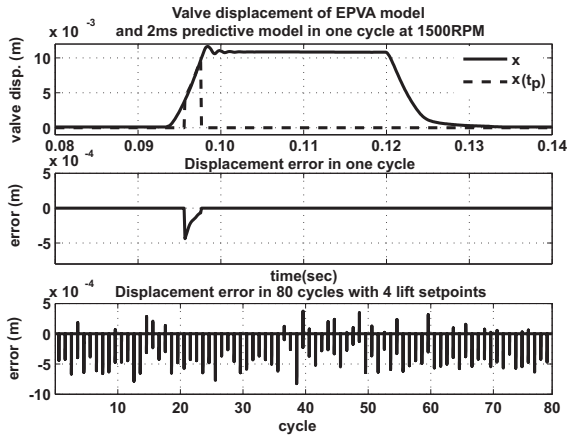

Fig. 9. Simulation validation of displacement prediction x_{0_p}

simulation results of the model-based velocity prediction are shown in Figure 10. The absolute error between the plant and predicted velocity is less than $0.25m/s$ over 80 simulated cycles using the closed-loop lift tracking control with four lift set points.

C. Simulation of Kalman Filter State Estimation

Figure 11 and Figure 12 present the simulation results of the Kalman filter state estimation with the measurement noise present. The top and middle graphs show one cycle response and the estimation error, and the bottom one shows the error over 80 engine cycles. The absolute error over 80 cycles between the plant displacement and the estimated displacement is less than $0.3mm$. The absolute error between the plant and estimated velocity is less than $0.38m/s$ over 80 simulated cycles using the closed-loop lift tracking control with four lift set points.

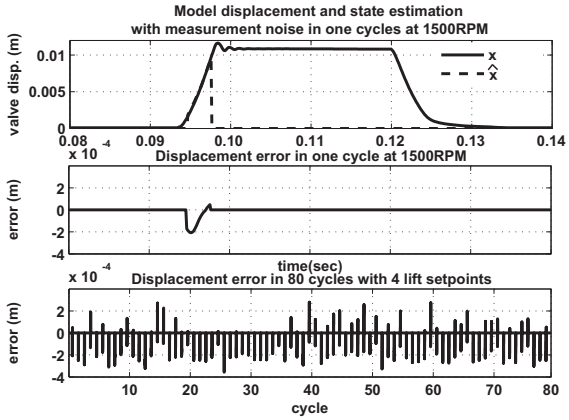

Fig. 11. Kalman filter displacement $(\widehat{x_0})$ estimation simulation

D. Simulation of Closed-Loop Exhaust Valve Lift Tracking

Finally, Figure 13 presents the entire closed-loop lift tracking simulation results with all three feedforward control sequences assembled at four reference lift set points in the presence of measurement noise. The dark and gray lines in the top diagram represent the reference and model valve lift respectively. The bottom diagram demonstrates that the absolute lift tracking error is below $0.6mm$ at steady state. The exhaust valve tracks the reference lift within one engine cycle with the lift error less than $0.6mm$.

It is clear that model-based predictive control is computationally intense. In order to reduce on-line calculation of PDC and ICP algorithms, off-line PDC simulations were conducted for a range of initial displacements and velocities. The simulation results were converted into lookup tables of displacement and velocity as inputs to ICP lookup table

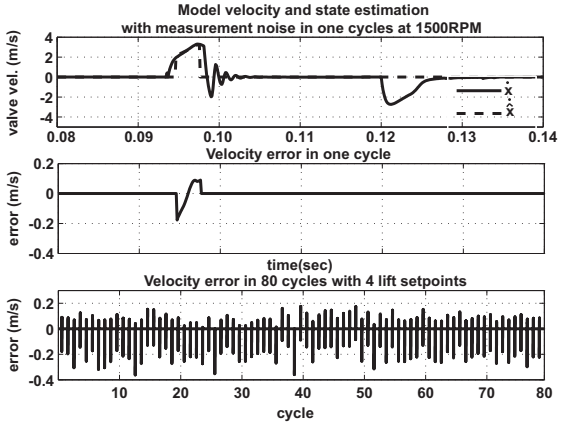

Fig. 12. Kalman filter velocity ($\widehat{x}_0$) estimation simulation

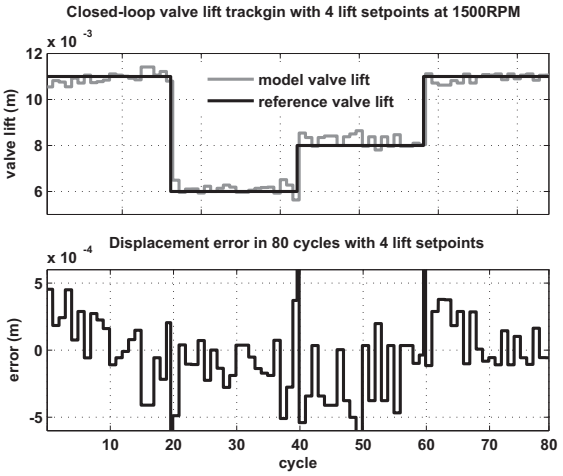

Fig. 13. Closed-loop lift tracking control with four set points

which is calibrated using off-line simulation data. Only the Kalman filter algorithm needs to run on-line. This strategy was implemented into a real-time controller with 40 microsecond sample rate [19].

V. CONCLUSION

A mathematical exhaust valve actuator model and an in-cylinder pressure model have been developed for a model-based predictive lift control of an exhaust valve. The exhaust valve model was approximated by a piecewise-linearized second order spring-mass-damper system. The in-cylinder pressure was modeled during the exhaust valve opening stage. This model was integrated with the exhaust valve actuator model for control development. The thermodynamics data used in this model was obtained with the WAVE^{TM} simulation which was calibrated using experimental in-cylinder pressure data. The in-cylinder pressure model was validated using experimental data and demonstrates satisfactory model accuracy.

A model-based predictive control strategy was developed for feedforward control. This strategy contains three segments; peak displacement calculation, model-based initial condition prediction and Kalman state estimation. Simulations were carried out with the white measurement noise to evaluate the performance of each individual segment and the integrated feedforward algorithm. A proportional and integral controller was used for closed loop control. The closed loop valve lift control system was integrated with model-based predictive feedforward control. Evaluation simulations were conducted at different reference lift set points with the white measurement noise based upon the developed exhaust valve and in-cylinder pressure models.

Simulation results show good robustness against measurement noise. The steady state valve lift error is below $0.6mm$ and the closed loop valve lift control system is able to track the step reference lift within one engine cycle with a lift error less than $0.6mm$.

REFERENCES

[1] K. Inoue, K. Nagakiro, Y. Ajiki, and N. Kishi, "A High Power Wide Torque Range Efficient Engine with a Newly Developed Variable Valve Lift and Timing Mechanism," *SAE 890675*, 1989.

[2] Y. Moriya, A. Watanabe, U. Uda, H. Kawanura, M. Yoshioka, and Adachi, "A Newly Developed Intelligent Variable Valve Timing System Continuously Controlled Cam Phasing as Applied to a New 3 Liter Inline 6 Engine," *SAE 960579*, 1996.

[3] R. Flierl and M. Kluting, "The Third Generation of New Fully Variable Valvetrain for Throttle Free Load Control," *SAE 2000-01-1227*, 2000.

[4] M. Theobald, B. Lequesns, and R. Henry, "Control of Engine Load via Electromagnetic Valve Actuators," *SAE 940816*, 1994.

[5] C. Boie, H. Kemper, L. Kather, and G. Corde, "Method for Controlling a Electromagnetic Actuator for Achieving a Gas Exchange Valve On a Reciprocating Internal Combustion Engine," *US Patent 6,340,008*, 2000.

[6] L. Schneider, "Electromagnetic Valve Actuator with Mechanical End Position Clamp or Latch," *US Patent 6,267,351*, 2001.

[7] I. Haskara, L. Mianzo, and V. Kokotovic, "Method of Controlling an Electromagnetic Valve Actuator," *US Patent 6,644,253*, 2003.

[8] Y. Wang, A. Stefanopoulou, K. Peterson, T. Megli, M. Haghgooie, "Modeling and Control of Electromechanical Valve Actuator," *SAE 2002-01-1106*, 2002.

[9] G. Wright, N. Schecter, and M. Levin, "Integrated Hydraulic System for Electrohydraulic Valvetrain and Hydraulicly Assisted Turbocharger," *US Patent 5,375,419*, 1994.

[10] O. Sturman, "Hydraulic Actuator for an Internal Combustion Engine," *US Patent 5,638,781*, 1994.

[11] Z. Sun and D. Cleary, "Dynamics and Control of an Electro-Hydraulic Fully Flexible Valve Actuation System," *Proceedings of American Control Conference*, Denver, Colorado, June, 2003.

[12] Jia Ma et al., "Analysis and Modeling of an Electronically Controlled Pneumatic Hydraulic Valve for an Automotive Engine," *SAE 2006-01-0042*, 2006.

[13] Jia Ma et al., "Model reference adaptive control of a pneumatic valve actuator for infinitely variable valve timing and lift," *2007 SAE World Congress (SAE 2007-01-1297)*, Detroit, MI, April, 2007.

[14] Jia Ma et al.,"Adaptive control of a pneumatic valve actuator for an internal combustion engine," *2007 American Control Conference*, New York, NY, July, 2007

[15] M. Anderson, T. C. Tsao, M. Levin, "Adaptive Lift Control for a Camless Electrohydraulic Valvetrain," *SAE 981029*, 1998.

[16] J. M. Tressler et al., "Dynamic Behavior of Pneumatic Systems for Lower Extremity Extenders," *Proceedings of the 2002 IEEE International Conference on Robotics & Automation*, Washington, D.C., May 2002.

[17] K. Misovec et al., "Digital Valve Technology Applied to the Control of an Hydraulic Valve Actuator," *SAE 1999-01-0825*, 1999.

[18] William T. Thomson, *Theory of vibration with applications* 5^{th} ed. Prentice Hall, Upper Saddle River, New Jersey, 1998.

[19] J. Ma, G. Zhu, T. Stuecken, A. Hartsig, and H. Schock, "Electro-pneumatic exhaust valve modeling and control for an internal combustion engine," *submitted to 2008 ASME ICE Spring Conference*, Chicago, IL, April, 2008

[20] http://www.ricardo.com/engineeringservices/software.aspx?page=wave